

# Catalysis Science & Technology

Accepted Manuscript



This is an *Accepted Manuscript*, which has been through the Royal Society of Chemistry peer review process and has been accepted for publication.

*Accepted Manuscripts* are published online shortly after acceptance, before technical editing, formatting and proof reading. Using this free service, authors can make their results available to the community, in citable form, before we publish the edited article. We will replace this *Accepted Manuscript* with the edited and formatted *Advance Article* as soon as it is available.

You can find more information about *Accepted Manuscripts* in the [Information for Authors](#).

Please note that technical editing may introduce minor changes to the text and/or graphics, which may alter content. The journal's standard [Terms & Conditions](#) and the [Ethical guidelines](#) still apply. In no event shall the Royal Society of Chemistry be held responsible for any errors or omissions in this *Accepted Manuscript* or any consequences arising from the use of any information it contains.

**Similarities and differences between aromatics-based and olefins-based cycles in H-SAPO-34 and H-SSZ-13 for methanol-to-olefins conversion: Insights from energetic span model**

Chuan-Ming Wang,\* Yang-Dong Wang, Yu-Jue Du, Guang Yang, Zai-Ku Xie\*

SINOPEC Shanghai Research Institute of Petrochemical Technology, Shanghai 201208, China

\*Tel. : (+86)21-68462197; Fax: (+86)21-68462283

E-Mail: [wangcm.sshy@sinopec.com](mailto:wangcm.sshy@sinopec.com), and [xzk@sinopec.com](mailto:xzk@sinopec.com)

**Abstract:**

Zeolites catalyzed methanol-to-olefins (MTO) conversion proceeds through hydrocarbon pool mechanism involving a series of elementary steps. The nature of active hydrocarbon pool species is yet to be clear in different zeolites. In this work, both aromatics-based and olefins-based cycles in H-SAPO-34 and H-SSZ-13 were systematically investigated using periodic DFT calculations with van der Waals (vdW) interaction corrected XC functional. Combining static adsorption energies and interconversion thermodynamics, we theoretically proved that 1,2,4,5-tetramethylbenzene (1,2,4,5-TMB) is the primary component of methylbenzenes in CHA-structured zeolites. The energetic span model was employed to compare the kinetics of both cycles in which 1,2,4,5-TMB and 2,3-dimethyl-2-butene (iso-C6) were taken as hydrocarbon pool species. Both cycles follow a similar sequence of elementary steps. We demonstrate that iso-C6-based cycle is kinetically facile for the MTO conversion in H-SAPO-34 and H-SSZ-13. The rate-determining transition states are identified as the propagation of side ethyl chain in 1,2,4,5-TMB-based cycle and the cracking in iso-C6-based cycle, respectively. Our results show that the reactivity of 1,2,4,5-TMB increases with acid strength from H-SAPO-34 to H-SSZ-13. The stabilities of carbenium ions, important intermediates in olefins-based cycle, increase with their size and zeolite acidity. These theoretical insights from energetic span model enable us to highlight the importance of olefins-based cycle in the MTO conversion and understand the dependence of the reaction mechanism on zeolite frameworks.

**Keywords:** methanol-to-olefins conversion; zeolite catalysis; density functional theory; aromatics-based cycle; olefins-based cycle; hydrocarbon pool; H-SAPO-34; H-SSZ-13.

## 1. Introduction

Sustainable production of fuels and chemicals is highly urgent in modern chemical industry. The interest in the use of methanol as source feedstock is rising as it can be produced from coal, natural gas, biomass, or CO<sub>2</sub>.<sup>1,2</sup> Among the processes for methanol conversion, methanol-to-olefins (MTO) conversion catalyzed by acidic zeolites or zeotypes, e.g. H-SAPO-34 and H-ZSM-5, provides a promising alternative to produce light olefins such as ethene and propene.<sup>3,4</sup> Last several decades have witnessed extensive investigations to improve catalyst performance and elucidate underlying reaction mechanism in both industrial and academic communities.<sup>5,6</sup>

Unraveling the MTO reaction mechanism is highly challenging due to the complexity in product distribution and the difficulty in the identification of active intermediates.<sup>7-11</sup> It is currently accepted that the MTO conversion follows a hydrocarbon pool (HP) mechanism from the joint experimental and theoretical investigations.<sup>12,13</sup> The active center consists of inorganic frameworks with Brønsted acidic site and organic active components known as HP species.<sup>14</sup> Aromatics like polymethylbenzenes (MBs) and/or olefins like higher olefins represent two kind of important HP species in the MTO conversion.<sup>15-20</sup> The evolution of both types of HP species constitutes two different cycles, known as dual-cycle concept.<sup>17-19</sup> In aromatics-based cycle, light olefins split off from side alkyl chains of cyclic compounds.<sup>8,9,21-24</sup> According to the formation route of side alkyl chains, two different routes (side chain vs. paring) were suggested.<sup>9,25</sup> In olefin-based cycle, a similar methylation and cracking pathway of aliphatic chains is followed.<sup>20,26-28</sup> It was found in H-ZSM-5 that ethene is exclusively produced from aromatics-based cycle, while propene and higher olefins are mainly produced via olefins-based cycle.<sup>17-19</sup> Understanding the structure dependence of HP species on zeolite frameworks and the relative contribution of each cycles would be crucial to control the MTO catalytic performance, in particular selectivity.

First-principles based theoretical calculation has exhibited its indispensable potential to unravel reaction mechanism and rationally design new catalysts for complex reactions.<sup>29-32</sup> In the case of theoretical studies on the MTO conversion, two different zeolite models were employed: cluster model and periodic model.<sup>31</sup> Both the calculated state energies (E-representation), and the rate-constants (k-representation) of elementary steps were exploited to address the reaction mechanism and understand the effect of frameworks.<sup>21-23,33-37</sup> However, inconsistency derived from both representations still remains based on the focus of viewpoint. For example, nature of active HP species is still unclear in

different zeolites. Recently, Shaik et al. proposed the energetic span model to build the connection between both representations for the efficient exploration of experimental and theoretical results.<sup>38</sup> In this work, the MTO reaction mechanism including aromatics-based and olefins-based cycles in H-SAPO-34 was theoretically revisited using the energetic span model at reaction temperature (673 K). Both catalytic cycles in H-SSZ-13 were further addressed to understand the effect of framework composition, i.e. acid strength. We demonstrate that both aromatics-based cycle and olefins-based cycle involve a similar sequence of elementary steps, and olefins themselves are active HP species. It is very necessary to use energetic span model to have a better understanding on complex reactions like the MTO conversion from theoretical point of view.

## 2. Computational methods and modeling

Both H-SAPO-34 and H-SSZ-13 were represented by a 36T hexagonal cell having one acidic site at the O2 position (see Figure 1). It should be mentioned that the interaction between organic species in different voids could be completely avoided using this periodic 36T model. All DFT calculations were performed using VASP software.<sup>39</sup> The projector augmented wave (PAW) was used to describe electron-ion interaction with the plane wave basis set kinetic energy cutoff equal to 400 eV.<sup>40,41</sup> The Bayesian error estimation functional with van der Waals (vdW) correlation (BEEF-vdW) was used.<sup>42</sup> The sampling of Brillouin zone was only with  $\Gamma$  point.<sup>43</sup> The dimer method was utilized to locate all transition states.<sup>44</sup> A force threshold of 0.01 eV/Å was employed for structure optimization of all intermediates and transition states. The lattice constants were optimized using 800 eV energy cutoff and 0.01 eV/Å force threshold (13.89, 13.89, 15.09 Å for AIPO-34, and 13.72, 13.72, 14.86 Å for CHA). All atoms in the cell were allowed to relax with the lattice constants being fixed. The harmonic frequency calculations employed a partial Hessian vibrational analysis (PHVA), including H atom of acidic site, and organic species part of involved states.<sup>45</sup> The zero point energies (ZPE), enthalpies, entropies, and Gibbs free energies were then calculated from harmonic frequencies. Accuracy of PHVA was checked via the comparison to full Hessian vibrational analysis (FHVA). Details can be found in Supplementary material, S1.

### 3. Results and discussion

#### 3.1 Adsorption and interconversion of MBs

Understanding the structure distribution of aromatics in zeolites is instructive to address the aromatics-based cycle and elucidate the deactivation behavior of catalysts.<sup>46</sup> Table 1 listed the adsorption enthalpies of different MBs in H-SAPO-34 and H-SSZ-13. Note that the adsorption of a hydrocarbon in zeolites usually depends on two opposite effects: Stabilization from dispersion interaction, and destabilization from steric repulsion interaction. The adsorption enthalpies of benzene are calculated to be around -70 kJ/mol in H-SAPO-34 and H-SSZ-13. The increase in adsorption enthalpies from benzene to xylenes implies that dispersion stabilization effect governs the interaction. The adsorption enthalpies of p-xylene (PX) are around -95 kJ/mol. For two different structures of trimethylbenzene (TriMB) and tetramethylbenzene (TMB) in H-SAPO-34 and H-SSZ-13, we found that their adsorption enthalpies differ more than 15 kJ/mol. The adsorption enthalpies of 1,3,5-TriMB and 1,2,3,5-TMB are even less than that of m-xylene, implying that both MBs start to suffer obvious steric constraints. 1,2,4,5-TMB is the MB that adsorbs strongest in H-SAPO-34 and H-SSZ-13 (~ 115 kJ/mol). With the increase in number of methyl groups, pentamethylbenzene (PMB) and hexamethylbenzene (HMB) experience strong repulsion interaction with CHA-structured framework. The vdW surface was shown in Figure S1 to qualitatively describe the interaction between MBs and H-SAPO-34 framework. Comparing the adsorption enthalpies of MBs in H-SAPO-34 and H-SSZ-13, we found that MBs without steric constraints (benzene, toluene, xylenes) adsorb slightly stronger in H-SSZ-13 than in H-SAPO-34, due to the smaller cavity size of H-SSZ-13 than H-SAPO-34. The adsorption of MBs with four or more methyl groups are weaker in H-SSZ-13 than in H-SAPO-34, in particular for HMB adsorption. The adsorption enthalpies of HMB in H-SSZ-13 and H-SAPO-34 are as low as -12 and -41 kJ/mol, respectively. The void of CHA-structured zeolites is therefore not spacious enough to accommodate HMB as a restricted-free HP species. It is surprising that the slight change in the void size may bring such noticeable difference of adsorption enthalpies in strong confined frameworks. The effect of channel size in the MTO conversion has also been observed in H-ZSM-12 and H-ZSM-22, and it is found that a slight size difference in channel may lead to dramatic difference in catalytic reactivity.<sup>47,48</sup>

The adsorption enthalpies of these MBs were also calculated using PBE functional and other methods (DFT-D2, DFT-D3, vdW-DF, and vdW-DF2) to correct vdW interaction (see

Supplementary material, Table S7).<sup>49-53</sup> The enthalpies of MBs were calculated to be similar (the differences are less than 10 kJ/mol) using BEEF-vdW, vdW-DF2 and DFT-D3 when the confinement effect of frameworks is not evident. However, they differ to a large extent in systems with strong confinement effect, such as HMB in H-SAPO-34 and H-SSZ-13. It raises an interesting question: how to accurately describe vdW interaction in strong confined frameworks?

In the MTO conversion, the interconversion between different MBs usually follows methylation step to change the number of methyl groups. In this work, the Gibbs free reaction energies at different temperatures from benzene to other MBs were calculated to understand the distribution of MBs in H-SAPO-34 (see Figure 2). Methanol and water in gaseous phase were included for energy reference. The primary component of MBs in zeolites is that exhibits the highest exothermicity from benzene.

At 0 K, the Gibbs free reaction energies from benzene to 1,2,4,5-TMB increase by about 70 ~ 80 kJ/mol for each methyl group. Due to the steric constraints, the Gibbs free reaction energies from benzene to PMB and HMB are similar (-300 ~ -320 kJ/mol). Approximate neutrality in reaction enthalpies from TMB to PMB and HMB in H-SAPO-34 indicates that both PMB and HMB suffer obvious confinement effect. With the increase in temperature, we found that Gibbs free reaction energies decrease in absolute value, and the free reaction energies of higher MBs are more sensitive to temperature than those of lower MBs. The contents of MBs in zeolites may shift to lower MBs with temperature increasing. As showed in Figure 2, we conclude that 1,2,4,5-TMB is the main constituent of MBs in H-SAPO-34 at 673 K. So is the case in H-SSZ-13, as the steric confinement effect is more severe in H-SSZ-13 than in H-SAPO-34 for HMB and PMB adsorption. This theoretical insight from both static adsorption and dynamic interconversion analysis agrees well with several experimental findings. Haw et al. found that the average number of methyl groups per ring reaches a maximum of about 4 during the reaction in H-SAPO-34.<sup>15</sup> Olsbye et al. observed in H-SAPO-34 that TMB and lighter MBs are the main constituent of MBs in retained hydrocarbons and only negligible amounts of HMB have been detected.<sup>54</sup> Recently, Davis et al. also found that TMB is the primary occluded species for the partially deactivated H-SSZ-13.<sup>55</sup> Liu et al. clearly identified that 1,2,4,5-TMB and PMB (with less concentration) are predominantly formed in H-SAPO-34.<sup>56</sup>

### 3.2 Evolution of aromatics-based and olefins-based cycles

Methanol adsorption at the acidic site is the initial step of the MTO reaction. The adsorbed structures in H-SAPO-34, H-SSZ-13 are presented in Figure 1. Methanol is physisorbed through hydrogen-bonding interaction with the frameworks. The protonated structures of methanol cannot be formed in both zeolites. As listed in Table 2, the adsorption enthalpies calculated using BEEF-vdW functional in H-SAPO-34 and H-SSZ-13 are -80 and -87 kJ/mol, respectively. Previous calculated adsorption results using different models or XC functionals were compared as listed in Table 2.<sup>57-59</sup> We also calculated these adsorption enthalpies using other XC functionals with/without vdW interaction correction (see Table 2). Methanol adsorbs stronger in H-SSZ-13 by about 10 kJ/mol than in H-SAPO-34 as a result of difference in acid strength.

Scheme 1 shows the detailed aromatics-based side chain hydrocarbon pool mechanism using 1,2,4,5-TMB as HP species in zeolites. The complete catalytic cycle consists of side alkyl chain propagation and side chain elimination.<sup>21-24</sup> The gem-methylation (TS1-2) of aromatics is the first step of this cycle, leading to the formation of polymethylbenzenium ions (polyMB<sup>+</sup>, in M2). The methylation of polymethylmethylenecyclohexadiene (PMMC) intermediates with exocyclic double bond dedicates to the side chain propagation (TS3-4, TS5-6). Several different elimination pathways were previously proposed.<sup>21,24</sup> Recently, an energetically facile pathway (M4/M6 → M10) was theoretically identified for the elimination of light olefins.<sup>22</sup> More details on the evolution of aromatics-based cycle can be found in previous literatures.<sup>22,23</sup> In the following section, the enthalpy barriers of elementary steps were briefly elucidated and compared to previous results.

In this work, the methylation step was studied through concerted pathway in which the adsorbed methanol reacts directly with double bond of intermediates. It should be mentioned that the preferred methylation mechanism still remains in debate,<sup>60-62</sup> and which may relate to reaction conditions due to the enthalpy-entropy trade-off: the stepwise pathway prevails at higher reaction temperatures and/or lower pressures while concerted pathway dominates at lower reaction temperatures and/or higher pressures. Despite of such debate, the preference of methylation pathway does not influence the conclusion of this work as the same reference state was used for comparison.

The Gibbs free energy diagram of complete 1,2,4,5-TMB-based cycle in H-SAPO-34 at 0 K and 673 K is given in Figure 3. The calculated enthalpy barriers at 0 K are 110, 82, and 102 kJ/mol for the first, second, and third methylation steps, respectively. These values are

similar to the energy-based barriers in 1,2,3,5-TMB-based cycle in H-SAPO-34 (114, 87, and 96 kJ/mol).<sup>23</sup> The enthalpy barriers of the formation of the exocyclic double bond by deprotonation are 53 and 97 kJ/mol mediated by water. The enthalpy barriers are less than 85 kJ/mol in three steps of the methyl shift along the carbon ring of carbenium ions with either side ethyl or iso-propyl chains (TS-MS1, TS-MS2, and TS-MS3). The elimination of the side ethyl and isopropyl chains (TS9-10) needs to overcome enthalpy barriers of about 81 and 39 kJ/mol respectively to produce ethene and propene. It is observed that the stability of benzenium ions increases with the length of side alkyl chains ( $M2 < M4 < M6$ ).

Figure 4 is the Gibbs free energy diagrams of HMB- and PX-based cycles revisited in H-SAPO-34 for the propagation of side ethyl chain. The deprotonation of polyMB<sup>+</sup> ions ( $M2 \rightarrow M3-W$ ) is not included as it is an endothermic step. The adsorption enthalpies of methanol are around -88 kJ/mol with the presence of HMB or PX, same to that in 1,2,4,5-TMB-based cycle. The enthalpy barriers of the gem-methylation and PMMC methylation are similar to previously calculated energy-based results using GPAW package ( $M1 \rightarrow TS1-2$ : 107 vs. 109 kJ/mol and 127 vs. 132 kJ/mol,  $M3-M \rightarrow TS3-4$ : 105 vs. 104 kJ/mol and 92 vs. 93 kJ/mol in HMB- and PX-based cycles).<sup>23</sup> The stability of polyMB<sup>+</sup> ions ( $M2$ ) is observed to increase with the number of substituted methyl groups. Heptamethylbenzenium (heptaMB<sup>+</sup>) ion is much stable than trimethylbenzenium ion by about 50 kJ/mol in H-SAPO-34. The stability of the corresponding neutral intermediate PMMC ( $M3-M$ ) is found to be less sensitive to the number of methyl groups. It should be noted that the gem-methylation of PX is highly endothermic, while the methylation of PX to form TriMB is exothermic. It is thus unlikely for PX as HP species to produce light olefins via aromatics-based cycle.

Olefins-based cycle is originated from the olefin methylation and cracking route proposed by Dessau three decades ago.<sup>20,26-28</sup> A complete reaction network was previously proposed based on the olefins-based cycle to rationalize the formation of olefins, alkanes, and aromatics.<sup>20</sup> In this work, we consider 2,3-dimethyl-2-butene (iso-C6) as HP species in zeolites. Using this specific HP species, the olefins-based cycle bears the resemblance to aromatics-based cycle using 1,2,4,5-TMB as HP species, enabling the direct comparison of the kinetics. As showed in Scheme 1, iso-C6-based cycle also includes a series of similar elementary steps, such as methylation (TS1-2, TS3-4, TS5-6), deprotonation (TS2-3, TS4-5), shift of methyl groups (TS-MS1) and alkyl chain cracking (TS9-10) to produce light olefins. In order to directly compare the kinetics of both cycles, the same (side) alkyl chain cracking step was employed with the assistance of water.

The Gibbs free energy diagram of iso-C6-based cycle including key elementary steps in H-SAPO-34 is showed in Figure 5. The deprotonation of carbenium ions and shift of methyl group are excluded for study as they are facile steps. At 0 K, the enthalpy barriers of the three elementary methylation steps are around 90 kJ/mol, lower than those in 1,2,4,5-TMB-based cycle. Both the formed carbenium ions (M2, M4, and M6) and higher olefins (M3-W, M5-W, MX) are increasing stabilized with the number of carbon atoms. But their sensitivities to the size are different. The stability difference between tertiary carbenium ions and corresponding olefins systematically decreases with the size (66 > 49 > 33 kJ/mol for C7, C8, and C9 chains); the higher olefins are still the most stable species in H-SAPO-34. The enthalpy barriers for the cracking of C8<sup>+</sup> and C9<sup>+</sup> ions to produce ethene and propene are 75 and 54 kJ/mol, respectively, similar to those in 1,2,4,5-TMB-based cycle (81 and 39 kJ/mol).

The 1,2,4,5-TMB-based cycle in H-SSZ-13 was also studied in this work to understand the effect of framework composition or acid strength. As showed in Figure 6, the enthalpy barriers of elementary gem-methylation (93 vs. 110 kJ/mol) and methylation of exocyclic double bond (70 vs. 82 kJ/mol) in H-SSZ-13 are lower than those in H-SAPO-34. Methanol adsorbs slightly stronger in H-SSZ-13 than H-SAPO-34 (-93 vs. -88 kJ/mol) with the presence of 1,2,4,5-TMB. The framework composition highly influences the stability of polyMB<sup>+</sup> ion (M2) (-85 vs. -57 kJ/mol). At 0 K, the overall enthalpy barrier of 1,2,4,5-TMB-based cycle in H-SSZ-13 is 131 kJ/mol, lower than that in H-SAPO-34 (142 kJ/mol).

The Gibbs free energy diagram of iso-C6-based cycle in H-SSZ-13 is showed in Figure 7. The methylation is more facile in H-SSZ-13 than in H-SAPO-34. The enthalpy barriers for three methylation steps are 71, 82 and 74 kJ/mol in H-SSZ-13. The stability difference between tertiary carbenium ions and olefins in H-SSZ-13 decrease with the size (43 > 26 > 9 kJ/mol for C7, C8, and C9 chains). The decrease of 16 – 17 kJ/mol for each carbon atom is similar in both H-SSZ-13 and H-SAPO-34. The carbenium ions is more stabilized in H-SSZ-13 than in H-SAPO-34 with the same size. The stability of carbenium ions would be more sensitive to its size and framework of zeolites. Due to the stabilization of framework on carbenium ions, the barriers of elementary cracking steps are higher in H-SSZ-13 than in H-SAPO-34 by about 10 kJ/mol (62 vs. 54 kJ/mol for propene elimination, 85 vs. 75 kJ/mol for ethene elimination). The optimized transition state structures of the elimination steps in both 1,2,4,5-TMB-based and iso-C6-based cycles are showed in Figure 8. Similar C-C breaking distances are observed in both cycles to produce ethene (2.6 Å) or propene (2.9 Å).

The distances of C-H breaking and O-H forming are around 1.3 ~ 1.4 Å.

### 3.3 Energetic span model analysis of aromatics-based and olefins-based cycles

We are now in a position to rationalize the calculated Gibbs free energy diagrams at MTO reaction temperature (673 K) for understanding the reaction mechanism and the nature of HP species in CHA-structured zeolites. Aromatics-based cycle in a large number of zeolites including H-SAPO-34, H-ZSM-5, and H-MCM-22 has been systematically studied using cluster or periodic models.<sup>21-24,35,36,63</sup> The rate constants of elementary steps were calculated and employed to identify the preferred reaction cycle and rate-determining steps. The calculated rate constants of the methylation and elimination steps in H-SAPO-34 and H-SSZ-13 are listed in Table 3. The methylation step, either on the gem-position of aromatics or the exocyclic double bond, is slower than the elimination steps to produce ethene or propene in aromatics-based cycle; this is in line with previous theoretical results in cluster H-SAPO-34 model.<sup>22</sup> Methylation activity of aromatics also increase with acid strength of zeolites, similar to the methylation of light olefins.<sup>45,64</sup> The methylation step of aromatics is previously considered as the key step in this cycle.<sup>22,56</sup> However, as many theoretical works indicated,<sup>23,36,63</sup> the deprotonation step to form PMMC intermediate with exocyclic double bond is highly endothermic. The formed PMMC intermediate is therefore unstable compared to the reactants. The concentration of PMMC intermediate would be very low, and which can usually be estimated using Boltzmann distribution relative to the lowest intermediate (M1, at 0 K) or reactants (M0, at 673 K); it was previously revealed by kinetic Monte Carlo simulation.<sup>36</sup> Desorption of water and adsorption of methanol for the methylation of exocyclic double bond also leads to extra entropy loss (~ 20 kJ/mol at 673 K). So just focusing on a single elementary step may not guarantee unbiased understanding of the calculated results in reactions with complex network.

In the energetic span model, Shaik et al. highlighted that the kinetics of the reaction cycle cannot be determined by single transition state.<sup>38</sup> They pointed out that the concept of rate-determining steps is misleading, and proposed the concept of rate-determining states. This model can be used to understand catalytic activity and selectivity for reactions involving complex network.

In 1,2,4,5-TMB-based cycle (see Figure 3), the rate-determining transition state is the methylation of exocyclic double bond to propagate side ethyl chain (TS3-4); the rate-determining intermediate is methanol in adsorption (M1, at 0 K) or in the gas phase

(M0, at 673 K). The energetic span can then be estimated according to the energies of both rate-determining states and their relative order in the cycle.<sup>38</sup> The energetic span, also termed as overall Gibbs free energy barriers, is around 200 kJ/mol in aromatics-based cycle in H-SAPO-34 at 673 K. HMB is not more reactive than TMB via aromatics-based cycle in H-SAPO-34, in line with energy-based calculations using periodic 12T model.<sup>23,36</sup>

In iso-C6-based cycle, the intermediate for methylation is higher olefins, and they are stable intermediates compared to the unstable PMMC in aromatics-based cycle. The alkyl chain cracking is the rate-determining transition state, and the most stable cracking precursor (higher olefin, or carbenium ion) is the rate-determining intermediate. As showed in Figure 5, C8 olefin (M5-W) is the rate-determining intermediate in iso-C6-based cycle eliminating both ethene and propene at 673 K in H-SAPO-34. While in H-SSZ-13 (see Figure 7), we found that tertiary C9<sup>+</sup> ion (M6) is even more stable than the corresponding C9 olefin at 673 K, and this ion is therefore the rate-determining intermediate for propene elimination. These results may imply that higher tert-carbenium ions could be experimentally identified in zeolites with stronger acid strength. It should be noted that the stabilities of the rate-determining transition state and intermediate vary with zeolite framework composition or topology. As mentioned in previous works,<sup>64-66</sup> the relative stabilities of carbenium ions or ion pair intermediates are more sensitive to acid strength than that of alkoxides and olefins.

As showed in Figure 3, because the side iso-propyl chain propagation is kinetically less favored compared to the ethene elimination, we conclude ethene is more selective than propene in aromatics-based cycle in H-SAPO-34 at 673 K. This reproduced previous theoretical results in H-SAPO-34 and experimental results in H-ZSM-5.<sup>17,22,23</sup> From the overall Gibbs free energy barriers (energetic span) of 1,2,4,5-TMB-based and iso-C6-based cycles (see Table 4), we found that iso-C6 seems to be more reactive than 1,2,4,5-TMB as HP species in H-SAPO-34 and H-SSZ-13. The energy span of iso-C6-based cycle is much less than that of 1,2,4,5-TMB-based cycle by about 40 kJ/mol in H-SAPO-34 at 673 K. In iso-C6-based cycle, ethene seems to be less selective than propene. In H-SSZ-13 with stronger acid strength, the energy span in both 1,2,4,5-TMB-based cycle and iso-C6-based cycle to produce ethene decreases by about 15 kJ/mol, while it increases slightly in iso-C6-based cycle to produce propene. So the selectivity to ethene may increase with the acid strength. It may explain the experimental findings that the ethene to propene ratio is higher in H-SSZ-13 than in H-SAPO-34.<sup>67</sup>

### 3.4 General discussion

In H-SPA0-34 catalyzed MTO conversion, it is experimentally reported that the ratio of propene to ethene is around 1, and the total selectivity to propene and ethene is over 80%.<sup>67</sup> To understand how the MTO conversion proceeds in H-SAPO-34, we should make the following findings clear. First, ethene is selectively favored than propene in aromatics-based cycle.<sup>17</sup> Second, propene is more active than ethene to participate in olefins-based cycle in methylation step.<sup>37,45</sup> Third, the diffusion of propene is severely restricted in CHA-structured framework.<sup>68</sup> Combining all these findings, it is more plausible that the olefins-based cycle is at least present in parallel with the aromatics-based cycle for the MTO conversion in order to explain the experimentally observed selectivity in H-SAPO-34. Utilizing NMR and DFT calculations, we recently identified some important intermediates (dienes, methylcyclopropanes) related to olefins-based cycle before the formation of aromatics, further highlighting the importance of olefins-based cycle in H-SAPO-34 catalyzed MTO conversion.<sup>69</sup>

PolyMB<sup>+</sup> ions, in particular heptaMB<sup>+</sup> ion, were experimentally identified to favor aromatics-based cycle.<sup>70,71</sup> These ions can be stabilized by increasing acid strength of zeolites or number of methyl groups. As shown in Figure 4, heptaMB<sup>+</sup> ion (M2) in H-SAPO-34 is only 5 kJ/mol less stable than co-adsorbed methanol and HMB (M1) at 673 K, suggesting that such kind of ions could be observed at MTO reaction temperature. However, as the methylation of PMMC with exocyclic double bond is rate-determining transition state in aromatics-based cycle, the identification of PMMC becomes important. To date, there are no direct experimental evidence to confirm the presence of PMMC.

In this work, we only consider iso-C6 as one example of HP species in olefins-based cycle and which involves a similar sequence of elementary steps with aromatics-based cycle. We should mention that the olefins-based cycle is not limited to iso-C6 as HP species because the methylation and isomerization of olefins are facile in zeolites.<sup>20</sup> Due to the complexity in the distribution of cracking precursors and cracking modes, we believe more energy-feasible pathways may exist to split off olefins in the MTO conversion. We previously demonstrated that the distribution of cracking precursors, which depends on zeolite structures and reaction conditions, influences reactivity and selectivity.<sup>20</sup> As a result, direct comparing the kinetics of olefins-based and aromatics-based cycles in different frameworks and reaction conditions is essential to rationally design zeolite catalysts and optimize operation conditions.

#### 4. Conclusion

To summarize, using periodic DFT calculations with vdW interaction corrected XC functional, we systematically investigated the aromatics-based and olefins-based cycles in H-SAPO-34 and H-SSZ-13. Both zeolites exhibit the same CHA framework topology with different framework composition. We found that 1,2,4,5-TMB is the major component of MBs in H-SAPO-34 and H-SSZ-13 from static adsorption and dynamic interconversion analysis, consistent with a series of experimental findings. 1,2,4,5-TMB and 2,3-dimethyl-2-butene were respectively considered as the HP species in aromatics-based and olefins-based cycles to build reaction networks involving similar sequence of elementary steps (methylation, deprotonation, methyl group shift in isomerization, and elimination/cracking). We demonstrate that the aromatics-based and olefins-based cycles are mechanically similar, as both cycles consist of (side) alkyl chain propagation and elimination steps. Because it is challenging to understand the calculated results in complex reactions, the energetic span model was employed to identify the preferred reaction mechanism and rate-determining states. We point out that in HSAPO-34 and H-SSZ-13 the side ethyl chain propagation is rate-determining in aromatics-based cycle; while in olefins-based cycle, the alkyl chain elimination/cracking is rate-determining. The direct comparison of energetic span in both cycles makes us place the olefins-based cycle on a strong foundation in zeolites catalyzed MTO conversion.

#### Acknowledgements

This work is financially supported by National Science Foundation of China (21103231, 91434102) and SINOPEC.

#### Supplementary information

Electronic supplementary information (ESI) available. See DOI:

#### References

- 1 G. A. Olah, *Angew. Chem. Int. Ed.*, 2005, **44**, 2636-2639.
- 2 M. Y. He, Y. H. Sun and B. X. Han, *Angew. Chem. Int. Ed.*, 2013, **52**, 9620-9633.
- 3 C. D. Chang and A. J. Silvestri, *J. Catal.*, 1977, **47**, 249-259.
- 4 C. D. Chang, *Catal. Rev. Sci. Eng.*, 1983, **25**, 1-118.

- 5 M. Stocker, *Micropor. and Mesopor. Mater.*, 1999, **29**, 3-48.
- 6 F. J. Keil, *Micropor. and Mesopor. Mater.*, 1999, **29**, 49-66.
- 7 U. Olsbye, S. Svelle, M. Bjorgen, P. Beato, T. V. W. Janssens, F. Joensen, S. Bordiga and K. P. Lillerud, *Angew. Chem. Int. Ed.*, 2012, **51**, 5810-5831.
- 8 J. F. Haw, W. G. Song, D. M. Marcus and J. B. Nicholas, *Acc. Chem. Res.*, 2003, **36**, 317-326.
- 9 U. Olsbye, M. Bjorgen, S. Svelle, K. P. Lillerud and S. Kolboe, *Catal. Today*, 2005, **106**, 108-111.
- 10 K. Hemelsoet, J. Van der Mynsbrugge, K. De Wispelaere, M. Waroquier and V. Van Speybroeck, *ChemPhysChem*, 2013, **14**, 1526-1545.
- 11 S. Ilias and A. Bhan, *ACS Catal.*, 2012, **3**, 18-31.
- 12 I. M. Dahl and S. Kolboe, *J. Catal.*, 1996, **161**, 304-309.
- 13 I. M. Dahl and S. Kolboe, *J. Catal.*, 1994, **149**, 458-464.
- 14 J. F. Haw and D. M. Marcus, *Top. Catal.*, 2005, **34**, 41-48.
- 15 W. G. Song, J. F. Haw, J. B. Nicholas and C. S. Heneghan, *J. Am. Chem. Soc.*, 2000, **122**, 10726-10727.
- 16 B. Arstad and S. Kolboe, *J. Am. Chem. Soc.*, 2001, **123**, 8137-8138.
- 17 S. Svelle, F. Joensen, J. Nerlov, U. Olsbye, K. P. Lillerud, S. Kolboe and M. Bjorgen, *J. Am. Chem. Soc.*, 2006, **128**, 14770-14771.
- 18 S. Svelle, U. Olsbye, F. Joensen and M. Bjorgen, *J. Phys. Chem. C*, 2007, **111**, 17981-17984.
- 19 M. Bjorgen, S. Svelle, F. Joensen, J. Nerlov, S. Kolboe, F. Bonino, L. Palumbo, S. Bordiga and U. Olsbye, *J. Catal.*, 2007, **249**, 195-207.
- 20 C. M. Wang, Y. D. Wang and Z. K. Xie, *J. Catal.*, 2013, **301**, 8-19.
- 21 C. M. Wang, Y. D. Wang, Z. K. Xie and Z. P. Liu, *J. Phys. Chem. C*, 2009, **113**, 4584-4591.
- 22 K. De Wispelaere, K. Hemelsoet, M. Waroquier and V. Van Speybroeck, *J. Catal.*, 2013, **305**, 76-80.
- 23 C. M. Wang, Y. D. Wang and Z. K. Xie, *Catal. Sci. Tech.*, 2014, **4**, 2631-2638.
- 24 D. Lesthaeghe, A. Horre, M. Waroquier, G. B. Marin and V. Van Speybroeck, *Chem. Eur. J.*, 2009, **15**, 10803-10808.
- 25 C. M. Wang, Y. D. Wang, H. X. Liu, Z. K. Xie and Z. P. Liu, *Micropor. and Mesopor. Mater.*, 2012, **158**, 264-271.
- 26 R. M. Dessau, *J. Catal.*, 1986, **99**, 111-116.
- 27 R. M. Dessau and R. B. Lapierre, *J. Catal.*, 1982, **78**, 136-141.
- 28 D. Lesthaeghe, J. Van der Mynsbrugge, M. Vandichel, M. Waroquier and V. Van Speybroeck, *Chemcatchem*, 2011, **3**, 208-212.
- 29 J. K. Nørskov, T. Bligaard, J. Rossmeisl and C. H. Christensen, *Nat. Chem.*, 2009, **1**, 37-46.
- 30 J. K. Nørskov, F. Abild-Pedersen, F. Studt and T. Bligaard, *Proc. Nat. Acad. Sci.*, 2011, **108**, 937-943.
- 31 V. Van Speybroeck, K. De Wispelaere, J. Van der Mynsbrugge, M. Vandichel, K. Hemelsoet and M. Waroquier, *Chem. Soc. Rev.*, 2014, **43**, 7326-7357.
- 32 C. M. Wang, R. Y. Brogaard, Z. K. Xie and F. Studt, *Catal. Sci. Tech.*, 2015, **5**, DOI: 10.1039/C1034CY01692K
- 33 D. Lesthaeghe, V. Van Speybroeck, G. B. Marin and M. Waroquier, *Angew. Chem. Int. Ed.*, 2006, **45**, 1714-1719.
- 34 D. Lesthaeghe, B. De Sterck, V. Van Speybroeck, G. B. Marin and M. Waroquier, *Angew. Chem. Int. Ed.*, 2007, **46**, 1311-1314.

- 35 B. Arstad, J. B. Nicholas and J. F. Haw, *J. Am. Chem. Soc.*, 2004, **126**, 2991-3001.
- 36 C. M. Wang, Y. D. Wang, H. X. Liu, Z. K. Xie and Z. P. Liu, *J. Catal.*, 2010, **271**, 386-391.
- 37 V. Van Speybroeck, J. Van der Mynsbrugge, M. Vandichel, K. Hemelsoet, D. Lesthaeghe, A. Ghysels, G. B. Marin and M. Waroquier, *J. Am. Chem. Soc.*, 2011, **133**, 888-899.
- 38 S. Kozuch and S. Shaik, *Acc. Chem. Res.*, 2010, **44**, 101-110.
- 39 G. Kresse and J. Furthmuller, *Phys. Rev. B*, 1996, **54**, 11169-11186.
- 40 G. Kresse and D. Joubert, *Phys. Rev. B*, 1999, **59**, 1758-1775.
- 41 P. E. Blochl, *Phys. Rev. B*, 1994, **50**, 17953-17979.
- 42 J. Wellendorff, K. T. Lundgaard, A. Møgelhøj, V. Petzold, D. D. Landis, J. K. Nørskov, T. Bligaard and K. W. Jacobsen, *Phys. Rev. B*, 2012, **85**, 235149.
- 43 H. J. Monkhorst and J. D. Pack, *Phys. Rev. B*, 1976, **13**, 5188-5192.
- 44 G. Henkelman and H. Jonsson, *J. Chem. Phys.*, 1999, **111**, 7010-7022.
- 45 R. Y. Brogaard, C. M. Wang and F. Studt, *ACS Catal.*, 2014, **4**, 4504-4509.
- 46 R. Y. Brogaard, B. M. Weckhuysen and J. K. Nørskov, *J. Catal.*, 2013, **300**, 235-241.
- 47 Q. Wang, Z.-M. Cui, C.-Y. Cao and W.-G. Song, *J. Phys. Chem. C*, 2011, **115**, 24987-24992.
- 48 Y. Y. Chu, X. Y. Sun, X. F. Li, L. H. Ding, A. M. Zheng and F. Deng, *Catal. Sci. Tech.*, 2015, **5**, DOI: 10.1039/C1035CY00312A.
- 49 J. P. Perdew, K. Burke and M. Ernzerhof, *Phys. Rev. Lett.*, 1996, **77**, 3865-3868.
- 50 S. Grimme, J. Antony, S. Ehrlich and H. Krieg, *J. Chem. Phys.*, 2010, **132**, 154104.
- 51 S. Grimme, *J. Comput. Chem.*, 2006, **27**, 1787-1799.
- 52 M. Dion, H. Rydberg, E. Schröder, D. C. Langreth and B. I. Lundqvist, *Phys. Rev. Lett.*, 2004, **92**, 246401.
- 53 K. Lee, É. D. Murray, L. Kong, B. I. Lundqvist and D. C. Langreth, *Phys. Rev. B*, 2010, **82**, 081101.
- 54 B. P. C. Hereijgers, F. Bleken, M. H. Nilsen, S. Svelle, K. P. Lillerud, M. Bjorgen, B. M. Weckhuysen and U. Olsbye, *J. Catal.*, 2009, **264**, 77-87.
- 55 Y. Bhowe, M. Moliner-Marin, J. D. Lunn, Y. Liu, A. Malek and M. Davis, *ACS Catal.*, 2012, **2**, 2490-2495.
- 56 J. Li, Y. Wei, J. Chen, S. Xu, P. Tian, X. Yang, B. Li, J. Wang and Z. M. Liu, *ACS Catal.*, 2015, **5**, 661-665.
- 57 C. Lo and B. L. Trout, *J. Catal.*, 2004, **227**, 77-89.
- 58 F. Bleken, S. Svelle, K. P. Lillerud, U. Olsbye, B. Arstad and O. Swang, *J. Phys. Chem. A*, 2010, **114**, 7391-7397.
- 59 K. Hemelsoet, A. Nollet, V. Van Speybroeck and M. Waroquier, *Chem. Eur. J.*, 2011, **17**, 9083-9093.
- 60 R. Y. Brogaard, R. Henry, Y. Schuurman, A. J. Medford, P. G. Moses, P. Beato, S. Svelle, J. K. Nørskov and U. Olsbye, *J. Catal.*, 2014, **314**, 159-169.
- 61 A. J. Jones and E. Iglesia, *Angew. Chem. Int. Ed.*, 2014, **53**, 12177-12181.
- 62 J. Van der Mynsbrugge, J. De Ridder, K. Hemelsoet, M. Waroquier and V. Van Speybroeck, *Chem. Eur. J.*, 2013, **19**, 11568-11576.
- 63 S. Wang, Z. Wei, Y. Chen, Z. Qin, H. Ma, M. Dong, W. Fan and J. Wang, *ACS Catal.*, 2015, 1131-1144.
- 64 C. M. Wang, R. Y. Brogaard, B. M. Weckhuysen, J. K. Nørskov and F. Studt, *J. Phys. Chem. Lett.*, 2014, **5**, 1516-1521.

- 65 H. Fang, A. Zheng, S. Li, J. Xu, L. Chen and F. Deng, *J. Phys. Chem. C*, 2010, **114**, 10254-10264.
- 66 H. Fang, A. Zheng, J. Xu, S. Li, Y. Chu, L. Chen and F. Deng, *J. Phys. Chem. C*, 2011, **115**, 7429-7439.
- 67 F. Bleken, M. Bjørgen, L. Palumbo, S. Bordiga, S. Svelle, K.-P. Lillerud and U. Olsbye, *Top. Catal.*, 2009, **52**, 218-228.
- 68 C. M. Wang, B. W. Li, Y. D. Wang and Z. K. Xie, *J. Energy Chem.*, 2013, **22**, 914-918.
- 69 W. Dai, C. Wang, D. Michael, G. Wu, N. Guan, L. Li, Z. Xie and M. Hunger, *ACS Catal.*, 2015, **5**, 317-326.
- 70 S. J. Kim, H.-G. Jang, J. K. Lee, H.-K. Min, S. B. Hong and G. Seo, *Chem. Commun.*, 2011, **47**, 9498-9500.
- 71 J. Li, Y. Wei, J. Chen, P. Tian, X. Su, S. Xu, Y. Qi, Q. Wang, Y. Zhou, Y. He and Z. Liu, *J. Am. Chem. Soc.*, 2011, **134**, 836-839.

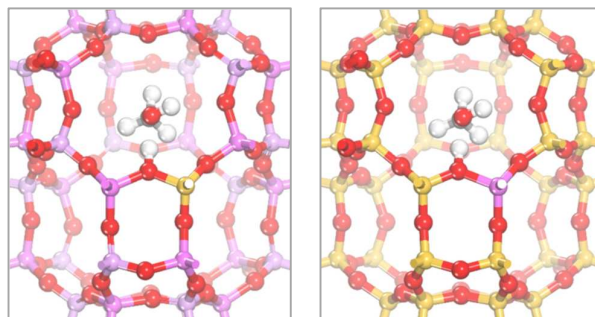


**Figure 1.** Adsorption structures of methanol in H-SAPO-34 (left) and H-SSZ-13 (right) simulated using periodic 36T model.

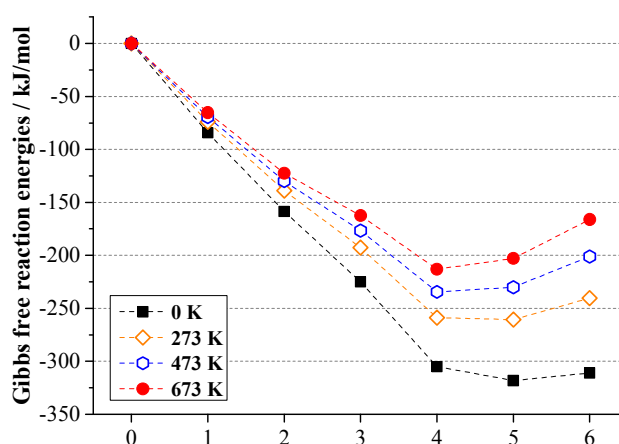


**Figure 2.** Gibbs free reaction energies of different MBs from benzene through repeated methanol methylation [Benzene +  $n \cdot \text{CH}_3\text{OH} \rightarrow \text{MB}(\text{CH}_3)_n + n \cdot \text{H}_2\text{O}$ ] in H-SAPO-34 at different temperatures. All energies are relative to gaseous methanol and water.

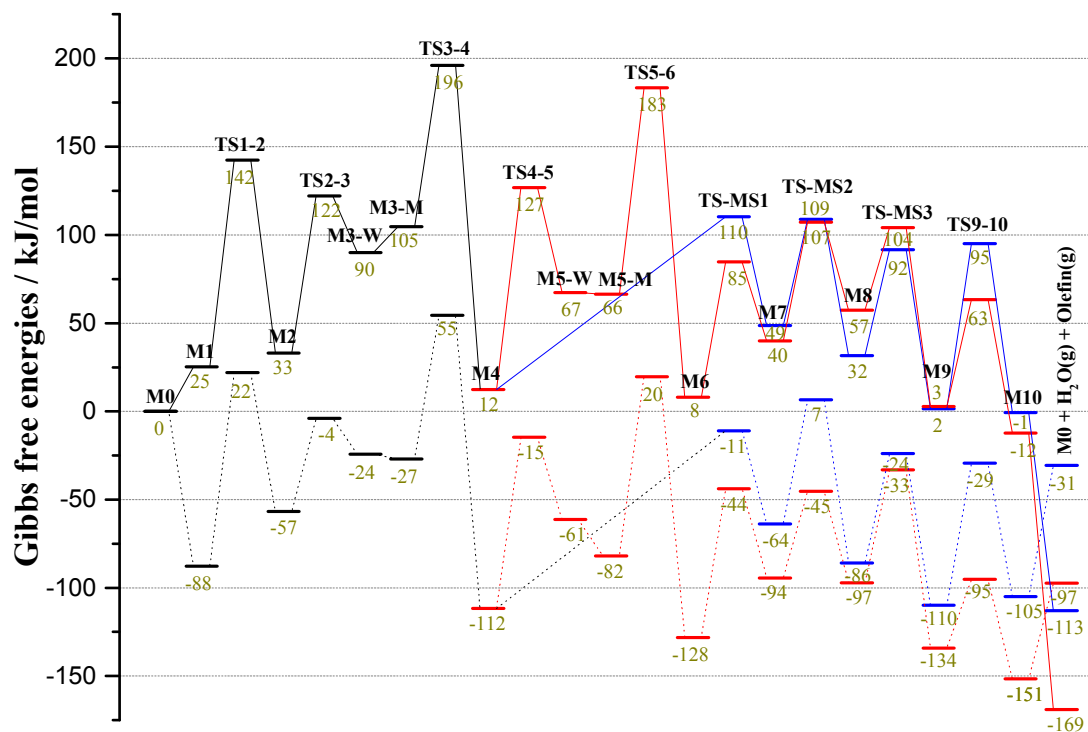


**Figure 3.** Gibbs free energy diagram of complete 1,2,4,5-TMB-based side chain hydrocarbon pool mechanism in H-SAPO-34 at 0 K (dotted line) and 673 K (solid line). The cycle consists of side ethyl chain propagation (in black), ethene elimination (in blue), and propene elimination (in red).

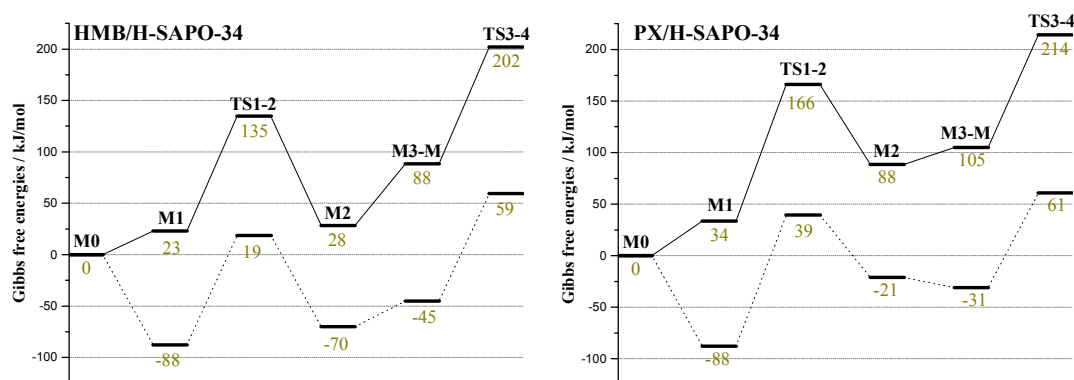


**Figure 4.** Gibbs free energy diagram of (left) HMB-, and (right) PX-based side chain hydrocarbon pool mechanism in H-SAPO-34 at 0 K (dotted line) and 673 K (solid line).

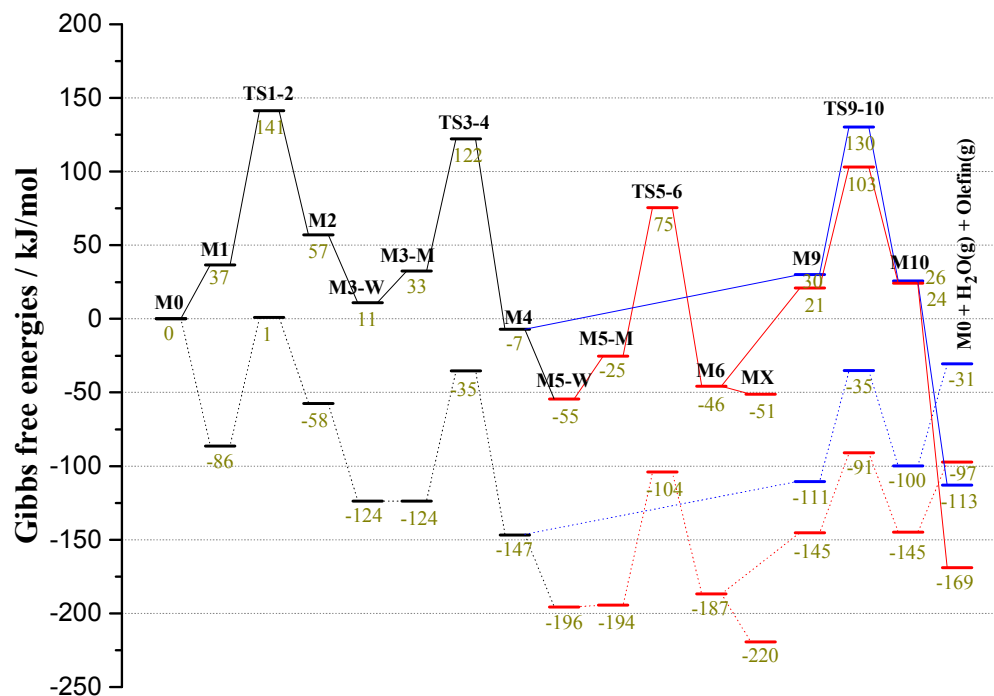


**Figure 5.** Gibbs free energy diagram of iso-C6-based hydrocarbon pool mechanism in H-SAPO-34 at 0 K (dotted line) and 673 K (solid line). The cycle consists of alkyl chain propagation (in black), ethene elimination (in blue), and propene elimination (in red).

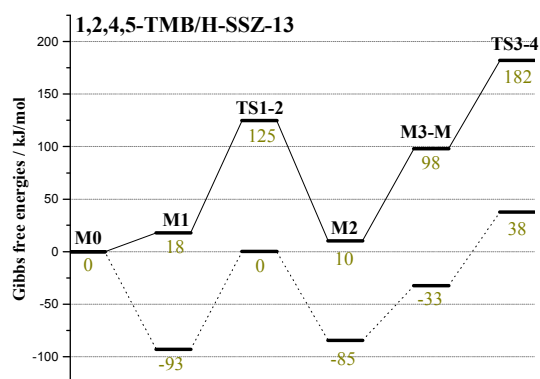


**Figure 6.** Gibbs free energy diagram of 1,2,4,5-TMB-based side chain hydrocarbon pool mechanism in H-SSZ-13 at 0 K (dotted line) and 673 K (solid line).

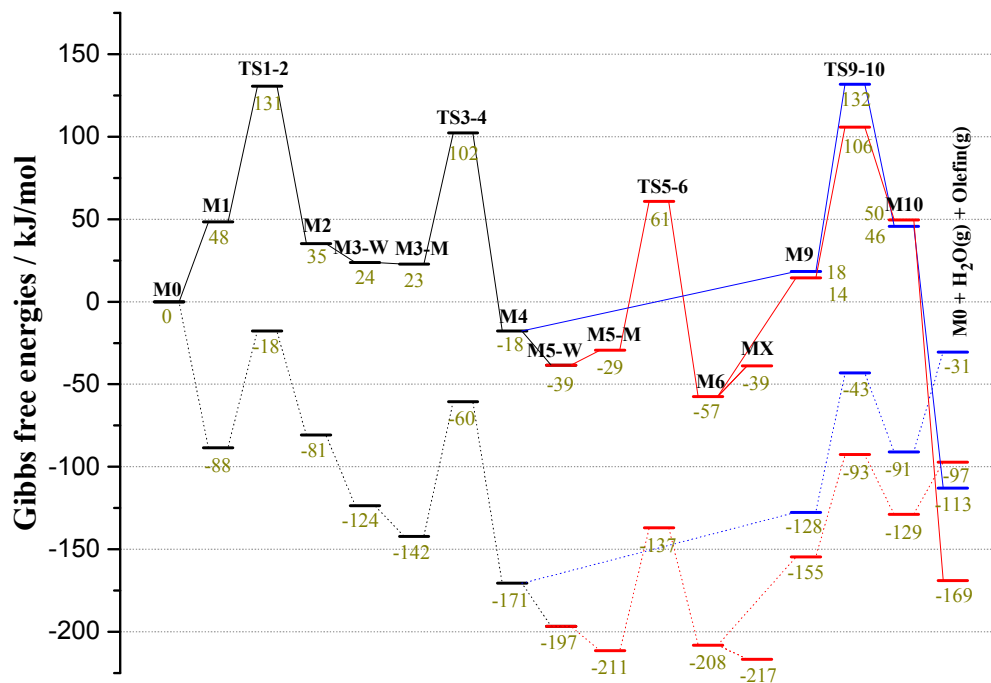


**Figure 7.** Gibbs free energy diagram of iso-C6-based hydrocarbon pool mechanism in H-SSZ-13 at 0 K (dotted line) and 673 K (solid line). The cycle consists of alkyl chain propagation (in black), ethene elimination (in blue), and propene elimination (in red).

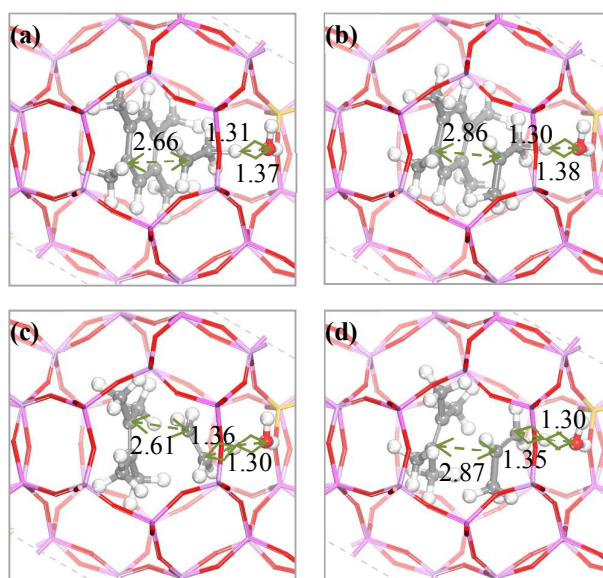


**Figure 8.** Optimized transition state structures splitting off ethene (left) and propene (right) in 1,2,4,5-TMB-based (top) and iso-C6-based (bottom) cycles in H-SAPO-34. The distances are given in Å.

**Table 1.** Adsorption enthalpies (kJ/mol) of MBs in H-SAPO-34 and H-SSZ-13 calculated using BEEF-vdW functional.

MBs	H-SAPO-34	H-SSZ-13
benzene	-69	-73
toluene	-88	-93
o-xylene	-97	-101
m-xylene	-90	-91
p-xylene	-96	-98
1,3,5-TriMB	-84	-84
1,2,4-TriMB	-99	-99
1,2,3,5-TMB	-86	-80
1,2,4,5-TMB	-116	-114
PMB	-87	-76
HMB	-41	-12

**Table 2.** Adsorption enthalpies (kJ/mol) of methanol in H-SAPO-34 and H-SSZ-13 calculated using different XC functionals. Previous calculated results by other researchers are included for comparison with ZPE correction (6 kJ/mol).

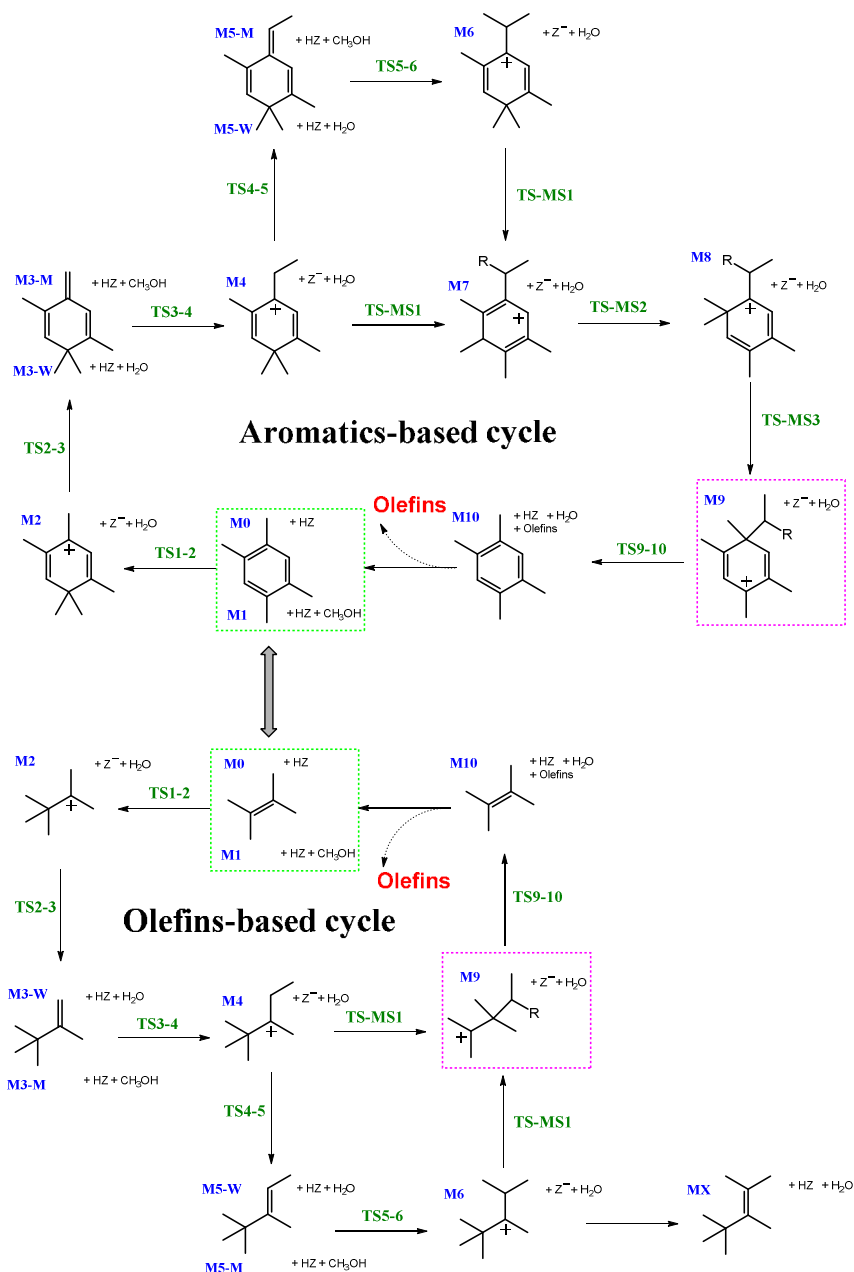
	H-SAPO-34	H-SSZ-13
BEEF-vdW	-80	-87
vdW-DF	-90	-98
vdW-DF2	-90	-98
DFT-D2	-101	-112
DFT-D3	-99	-109
PBE	-65	-74
Trout et al. <sup>57</sup>		-85 ~ -88
Swang et al. <sup>58</sup>	-75	-92
Van Speybroeck et al. <sup>59</sup>	-84	-104

**Table 3.** Gibbs free energy barriers ( $\Delta G^{\ddagger}_{\text{int}}$ , kJ/mol) and rate constants ( $k$ , s<sup>-1</sup>) for the methylation and elimination steps in 1,2,4,5-TMB-based and iso-C6-based cycles in H-SAPO-34 and H-SSZ-13 at 673 K.

	$\Delta G^{\ddagger}_{\text{int}}$				$k$			
	H-SAPO-34		H-SSZ-13		H-SAPO-34		H-SSZ-13	
	TMB	iso-C6	TMB	iso-C6	TMB	iso-C6	TMB	iso-C6
TS1-2	117	105	107	82	$1.1 \times 10^4$	$1.0 \times 10^5$	$7.1 \times 10^4$	$5.7 \times 10^6$
TS3-4	91	90	84	79	$1.2 \times 10^6$	$1.5 \times 10^6$	$4.0 \times 10^6$	$9.7 \times 10^6$
TS5-6	117	101		90	$1.2 \times 10^4$	$2.1 \times 10^5$		$1.4 \times 10^6$
TS9-10/C2	94	100		113	$7.7 \times 10^5$	$2.4 \times 10^5$		$2.2 \times 10^4$
TS9-10/C3	60	82		91	$2.8 \times 10^8$	$6.1 \times 10^6$		$1.1 \times 10^6$

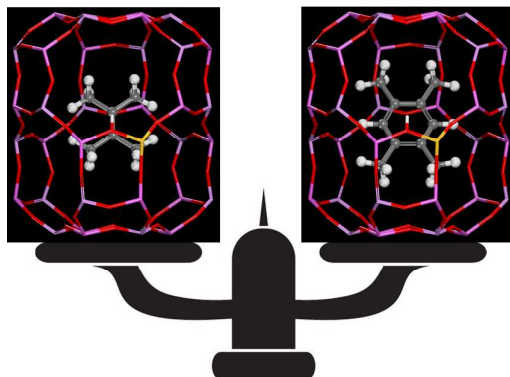
**Table 4.** The overall Gibbs free energy barriers ( $\Delta G^{\ddagger}$ , energetic span, kJ/mol) of 1,2,4,5-TMB-based and iso-C6-based cycles in H-SAPO-34 and H-SSZ-13 at 0 K and 673 K.

	$\Delta G^{\ddagger}_{0\text{ K}}$		$\Delta G^{\ddagger}_{673\text{ K}}$	
	H-SAPO-34	H-SSZ-13	H-SAPO-34	H-SSZ-13
1,2,4,5-TMB-based cycle	142	131	196	182
iso-C6-based cycle to C3	129	124	157	163
iso-C6-based cycle to C2	161	154	185	170



**Scheme 1.** Similarities between aromatics-based and olefins-based cycles in zeolites (HZ) for the MTO conversion.<sup>22,23</sup> 1,2,4,5-TMB and iso-C6 were taken as examples of HP species in both cycles. The adsorption of HP species in zeolites (M0) is the starting state for energy reference as they cannot diffuse away from voids in CHA-structured zeolites. Besides confined organic species, the adsorbed methanol or water, and zeolites (HZ or Z<sup>-</sup>), which are depicted as superscript or subscript at the right of each organic species, constitutes the calculated intermediate states of the cycle. Methanol for the growth of side alkyl chains was introduced through substituting adsorbed water at acidic site.

## TOC



Both aromatics-based and olefins-based cycles involve similar sequence of elementary steps. Energetic span model analysis indicates olefins are active hydrocarbon pool species in H-SAPO-34 and H-SSZ-13 for the methanol-to-olefins conversion.